Computational design of high-affinity protein binders targeting the HSV-1 viral protein UL12.5

Pien Siermann

S5063469

Supervised by: Karim Rafie

07 April 2025

ABSTRACT

Herpes simplex virus type 1 (HSV-1) is a highly prevalent pathogen. While most infections are either asymptomatic or cause oral sores, the virus poses serious health risks, particularly for immunocompromised individuals. Current treatment strategies are ineffective against HSV-1 in its latent state, allowing for viral reactivation and recurrence. The HSV-1 viral UL12.5 protein plays a key role in mitochondrial DNA (mtDNA) degradation and contributes to viral reactivation. This research project focuses on designing *de novo* protein binders that target UL12.5, with the goal of developing a novel therapeutic strategy to prevent HSV-1 reactivation and recurrence. Using a computational approach 1500 proteins binders against UL12.5 were designed. Unfortunately, none of the designed binders were identified to be high-affinity binders, and are therefore unlikely to prevent UL12.5 from degrading mtDNA or prevent the recurrence of active infection. Future studies could improve by targeting the designed binders towards specific binding spots essential for UL12.5's activity. Once these binders are shown to bind to UL12.5 with high-affinity, their ability to prevent mtDNA degradation and recurrence can be evaluated through *in vitro* and *in cellulo* experiments, contributing to the development of novel therapeutics against HSV-1.

INTRODUCTION

Herpes simplex virus type 1

Herpes Simplex Virus Type 1 (HSV-1) infects approximately 70% of the human population making it a highly prevalent pathogen, which is primarily transmitted through body fluids, especially saliva [1]. HSV-1 infects mucosal surfaces and can therefore infect the mouth, lips, lungs, eyes, metabolic system, central nervous system and genitals [2]. Initial infection of HSV-1 often presents as primary herpetic gingivostomatitis (PHGS), which is characterised by painful sores around the mouth [1, 2]. The severity of symptoms can vary, depending strongly on the immune system of the host and the speed at which the virus established latency. Notably, most HSV-1 infections are asymptomatic, and in some cases lead to non-specific symptoms such as muscle aches. Due to the hidden nature of HSV-1 infections, many cases go undiagnosed, contributing to the continued spread of the virus.

HSV-1 is a nuclear-replicating, enveloped virus with a spherical shape, ranging between 120 and 150 nm in diameter. The viral particle structure is composed of three main components: (1) an icosahedral protein capsid containing the viral genome, which consists of linear double stranded DNA molecules (2) a lipid bilayer envelope embedded with glycoproteins essential for cell entry, and (3) the tegument, a protein-filled compartment that facilitates the initiation of the infection [3].

Initial replication of HSV-1 occurs in the mucosal surfaces. From there, it enters sensory nerve endings and migrates into nerve cells. Replication within these neuronal cell bodies is limited, causing it to become latent. During latency, the virus remains dormant within neuronal reservoirs in a non-replicating, non-pathogenic state. However, in response to certain stimuli (e.g. physiological stress, fever, UV exposure or menstruation [4]) the virus can reactivate, leading to recurrent symptomatic infections. The reactivation of HSV-1 consists of two phases: (1) an initial burst of lytic gene expression, followed by (2) activation of viral genes during lytic replication, and therefore production of infectious virus [5]. While these recurrent infections are often milder than the initial outbreak, reactivation in immunocompromised patients can cause serious morbidities and even mortality. In rare cases infection of the central nervous system can lead to brain infections [1, 4, 5].

UL12.5 and its role in reactivation

HSV-1 contains the UL12 gene that encodes for an enzyme that has both endo- and exonuclease alkaline DNase activity [6]. This gene produces two proteins: (1) full-length UL12, which localises to the nucleus and plays a crucial role in viral genome maturation, and (2) UL12.5, an amino-terminally truncated variant that initiates at codon 127 of UL12 (figure 1). Unlike UL12, UL12.5 is primarily localised in the mitochondria, where it facilitates mitochondrial genome (mtDNA) degradation. Degradation of mtDNA results in dysfunction of the host cell functions, since mitochondria play a crucial role in the energy metabolism, innate immune response, RNA translation and programmed cell death [7]. HSV-1-induced mtDNA degradation has therefore been linked to several pathological conditions such as neuropathy and myopathy [6].

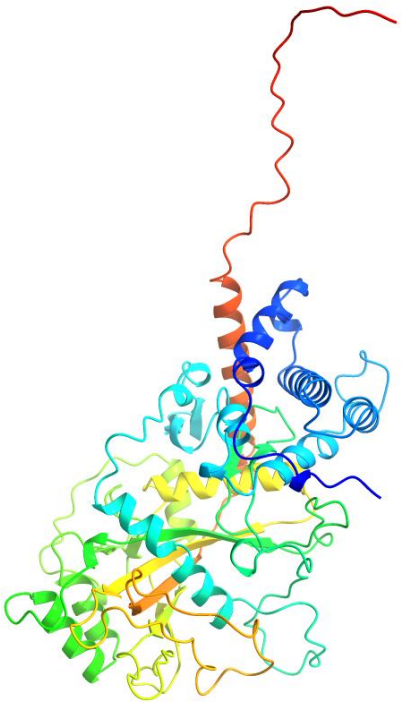

Figure 1 Predicted structure of UL12.5 as a cartoon model, colored in rainbow gradient from blue at the N-terminus to red at the C-terminus, visualised using ChimeraX

Given that HSV-1 can reach neuronal tissue, including the brain, the latent reservoirs and recurrence of active infection contributes to neuronal damage. Recent studies show that the neuronal damage caused by HSV-1 resembled the neuronal damage of Alzheimer's disease (AD) [8].

During lytic infection, mtDNA degradation triggers the cGAS-STING pathway, which enhances innate immune responses in mitotic cells and restricts viral replication. However, in postmitotic neurons, where HSV-1 establishes latency, cGAS-STING activation stimulates phase I of reactivation, increasing lytic gene expression and facilitating viral reactivation [5].

Limitations to current treatment therapies

The primary approach of treating HSV-1 infections relies on antiviral drugs. However, a significant challenge with these therapies is the development of drug resistance due to mutations. Furthermore, antiviral drugs such as nucleoside analogues —the most commonly used treatment for HSV-1 infection— inhibit the viral DNA polymerase. Consequently, the DNA polymerase of the host is also affected to some extent, contributing to the higher toxicity of these drugs [2, 9]. Another major limitation of antiviral drugs is that they fail to target the latency or reactivation process, allowing for lifelong viral persistence and recurrent outbreaks [2, 10].

Targeting UL12.5 as a novel therapeutic strategy

Given its critical role in HSV-1 reactivation, UL12.5 is a promising therapeutic target for preventing viral recurrence. This bachelor's research project aims to design high-affinity protein binders *de novo* against UL12.5 using computational protein design workflows, such as RFdiffusion and ProteinMPNN. By blocking UL12.5, this approach could offer an alternative treatment option that works differently from current antiviral drugs and may help overcome some of their limitations.

MATERIALS AND METHODS

A computational *de novo* protein design pipeline was used to predict high-affinity binders for UL12.5 (predicted structure provided by Karim Rafie) [11]. All these steps up to the AlphaFold2 (AF2) prediction were performed on the High Performance Cluster (HPC) Hábrók from the University of Groningen.

First, the full structure of the UL12.5 protein was fed into RoseTTAFold diffusion (RFdiffusion). RFdiffusion is a program which is able to predict the backbone structure of protein binders and generating protein data base (PDB) files [11]. The diffusion script was set to design 1500 binders, each ranging between 80 and 120 amino acids long, covering all 500 residues of UL12.5.

As a second step, the output of RFdiffusion was fed into ProteinMPNN-Fastrelax, which generates amino acid sequences that could fold into the designed backbone structures [12].

Finally, AF2 was used to predict the three-dimensional structure of the designed protein binders [13]. To assess the confidence of these predictions, we used the predicted Aligned Error (pAE) interaction score calculated by AF2 [14, 15]. In this experiment, we applied a pAE interaction cut-off value of 10 to identify high-affinity binders [16]. A scatterplot was generated using Microsoft Excel to visualise and identify binders with the lowest pAE scores, representing the most promising binders.

The protein design pipeline generates PDB files of the predicted structures of each designed protein binder. The interactions between the predicted structure of UL12.5 and the predicted structure of designed binders were analysed using ChimeraX [17].

RESULTS

The *de novo* protein design pipeline was set to design binders across the entire predicted structure of UL12.5. Figure 2 illustrates the interaction scores of all 1500 binders (the raw data of these binders can be found in the appendix). A lower pAE score indicates higher confidence in the spatial relationships between residues, suggesting a stronger interaction between the binder and UL12.5 [16]. The designed protein binders scored between 14,042 and 28,779, with the majority of the binders having a pAE score above 25 and none of them having a pAE interaction score below the cut-off value of 10 (indicated by the dotted line). Despite this, the interactions with UL12.5 and structures of the top three binders, as shown in table 1 were analysed using ChimeraX.

Table 1 Top 3 designed protein binders with the lowest pAE interaction score targeting UL12.5

binder number	pAE interaction score
878	14,042
766	15,763
136	16,682

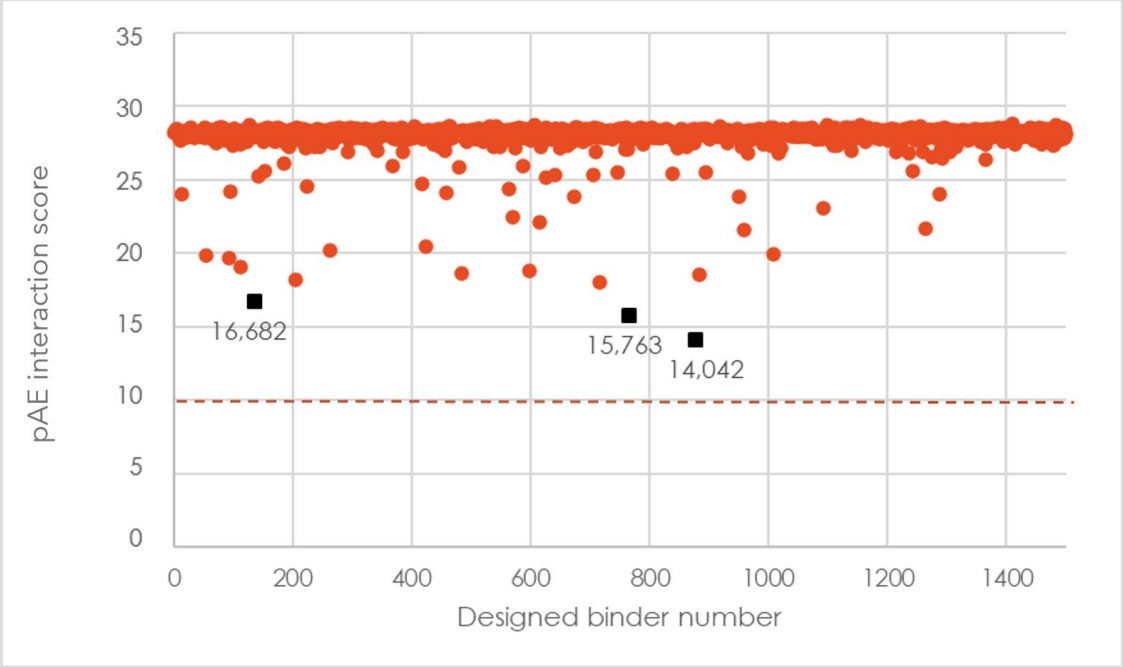

Figure 2 Scatterplot of all 1500 binders designed against UL12.5, represented as red dots, with their corresponding pAE interaction scores. The three binders with the lowest pAE interaction scores are highlighted as black squares. The red dotted line marks the cut-off value (10)

These three binders together with UL12.5 (white) can be seen in figure 3. Binder #878 (orange) and #766 (red) bind at a different side of UL12.5 compared to binder #136 (dark red).

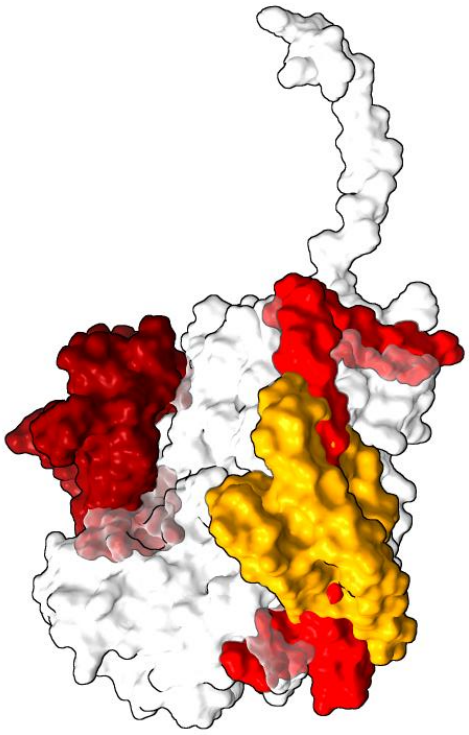

Figure 3 The predicted structure of UL12.5 (white) together with binders #878 (orange), #766 (red) and #136 (dark red), represented as a surface model using ChimeraX

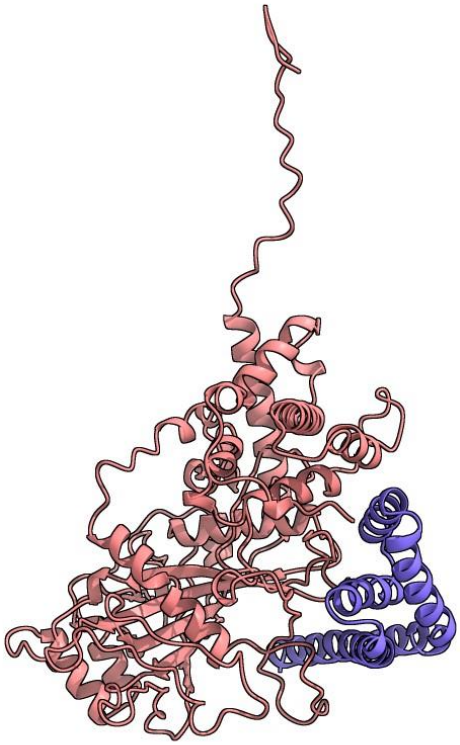

Figure 4 The predicted structure of UL12.5 as a cartoon model (pink) together with binder #878 (purple), visualised using ChimeraX

The predicted structure of binder #878 (purple), which had the lowest interaction score together with the predicted structure of the full length UL12.5 (pink), is illustrated in figure 4. Binder #878 consists of several alpha helices, that pack onto each other to form a small globular protein binding onto UL12.5.

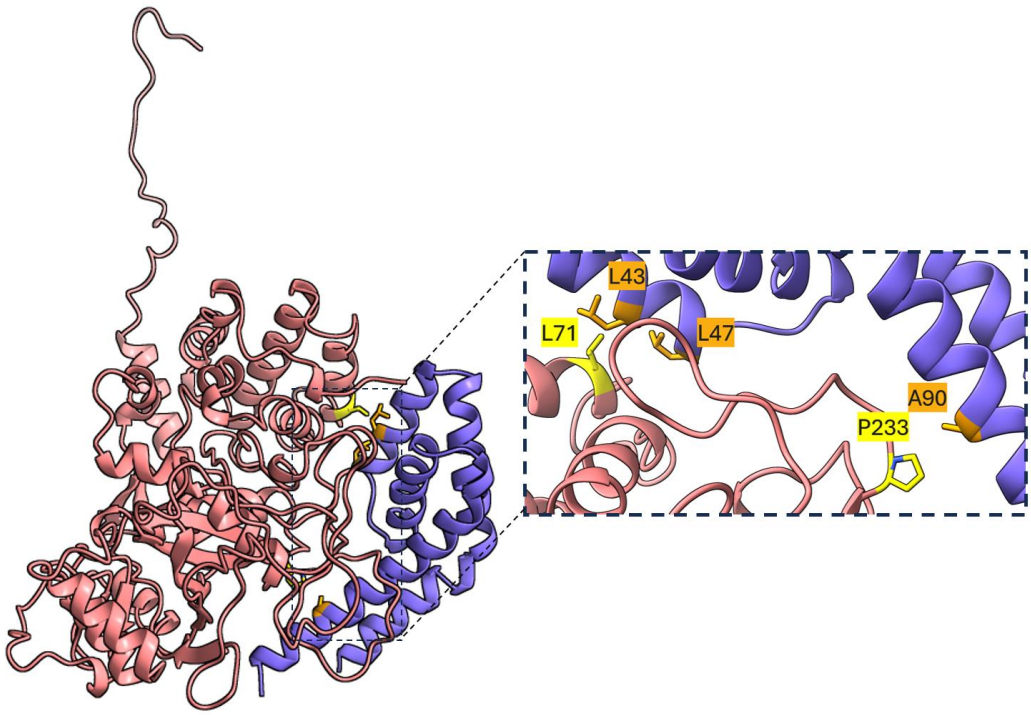

Figure 5 The predicted structure of UL12.5 as a cartoon model (pink) together with binder #878 (purple), with highlighted atoms of residues L43, L47, A90 (orange) and L73, P233 (yellow) to show potential hydrophobic interactions, visualised using ChimeraX

Possible hydrophobic interactions between hydrophobic residues are shown in figure 5. There are potential hydrophobic interactions between two leucine residues on the binder ($L43_{binder}$ and $L47_{binder}$) with leucine on UL12.5 ($L71_{UL12.5}$) and another interaction between alanine ($A90_{binder}$) with proline ($P233_{UL12.5}$). The distance between the interacting hydrophobic residues were all approximately 4.0 Å.

In figure 6 the predicted structure of binder #766 (purple) with UL12.5 (pink) can be seen. The binder adopts a long alpha helix positioned parallel with the full length of the target protein.

The N-terminus of binder #766 threads through UL12.5, as shown in figures 7 and 8. This region of the binder has a positive electrostatic potential (figure 7), while UL12.5 has more negative charge (figure 8). In the part of the binder that loops through UL12.5 a potential hydrogen bond is found, as illustrated in figure 9.

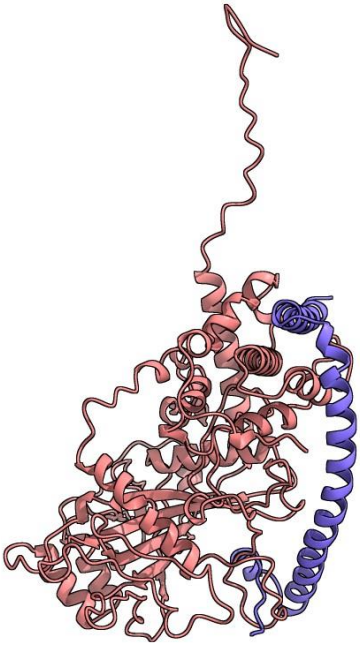

Figure 6 The predicted structure of UL12.5 as a cartoon model (pink) together with binder #766 (purple), visualised using ChimeraX

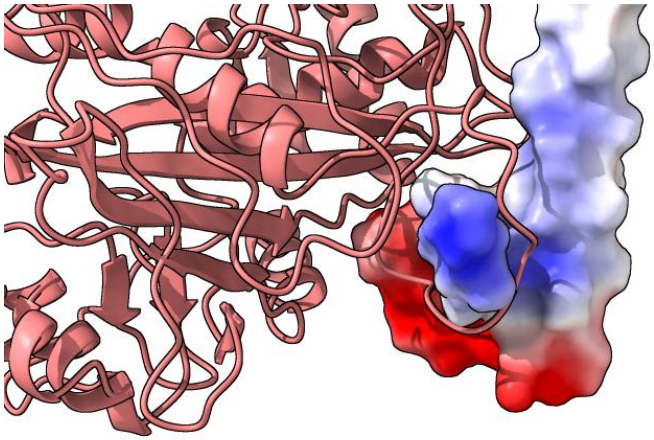

Figure 7 The predicted structure of UL12.5 as a cartoon model (pink) together with the electrostatic potential surface with negative potential in red, neutral potential in white and positive potential in blue of binder #766 (purple), visualised using ChimeraX

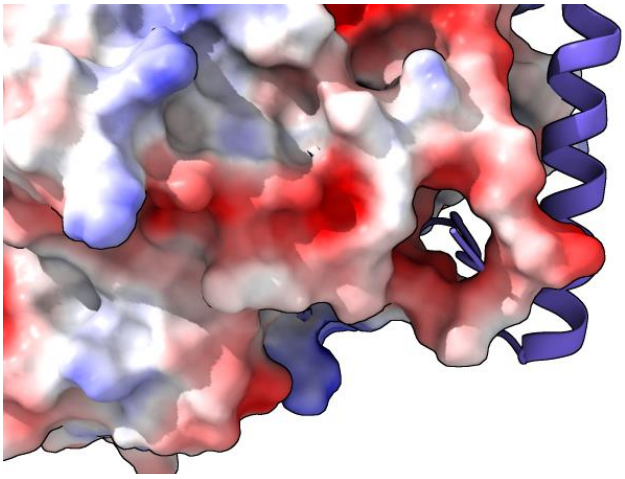

Figure 8 The predicted electrostatic potential surface with negative potential in red, neutral potential in white and positive potential in blue of UL12.5 together with the cartoon representation of binder #766 (purple),visualised using ChimeraX

The proline residue at location $P1_{binder}$ at the N-terminus of the binder can form a potential hydrogen bond with glutamic acid at location $E174_{UL12.5}$ on UL12.5 The distance of this hydrogen bond is 1.982 Å.

Additionally, there are some possible electrostatic interactions between the binder and UL12.5, which are depicted in figure 10.

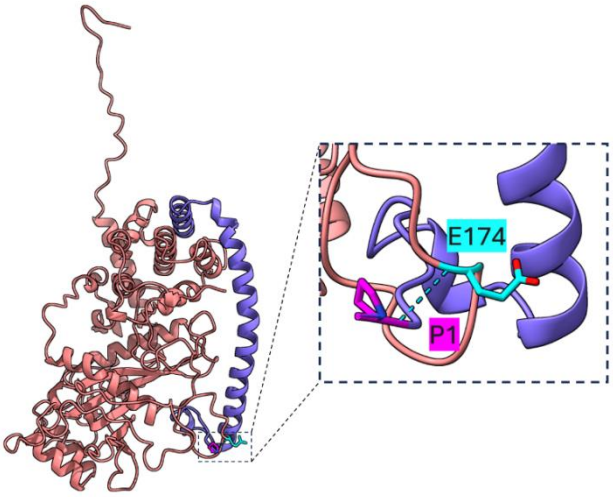

Figure 9 The predicted structure of UL12.5 as a cartoon model (pink) together with binder #766 (purple), with highlighted atoms of residues P1(magenta) and E174 (cyan) to show a potential hydrogen bond (dashed blue line), visualised using ChimeraX

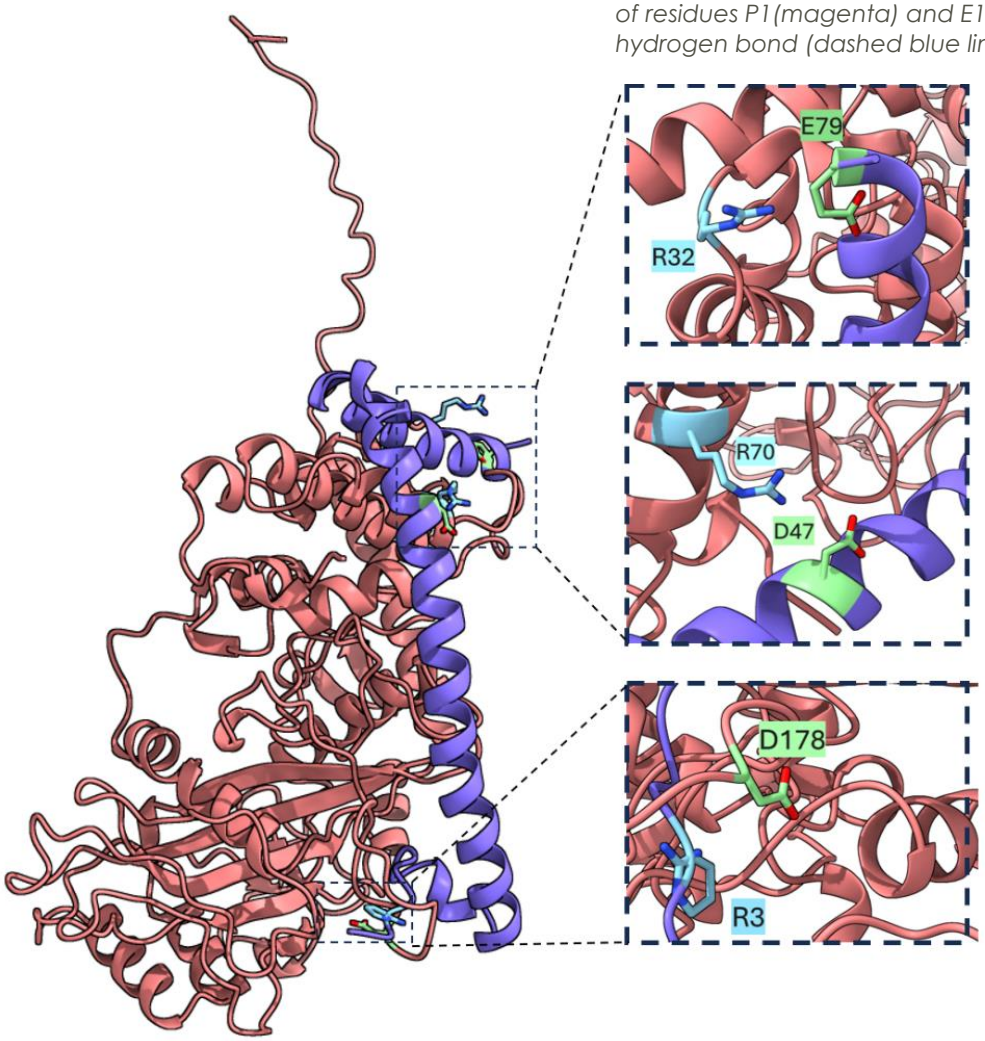

Figure 10 The predicted structure of UL12.5 as a cartoon model (pink) together with binder #766 (purple), with highlighted atoms of residues R32, R70, R3 (blue) and E79, D47, D178 (green) to show potential electrostatic interactions, visualised using ChimeraX

Figure 10A shows the positive residue arginine ($R32_{UL12.5}$) and the negatively charged glutamic acid ($E79_{binder}$) near the C-terminus of the binder that can engage in an electrostatic interaction, while figure 10B is focused on the possible interaction

between arginine ($R70_{UL12.5}$) with aspartic acid ($D47_{binder}$). Lastly, in the part where the binder loops through UL12.5 the negative aspartic acid residue($D178_{UL12.5}$) can engage in an electrostatic interaction with the positively charged arginine ($R3_{binder}$), as illustrated in figure 10C. The distance between interacting residue pairs spans from 4.4 to 6.0 Å.

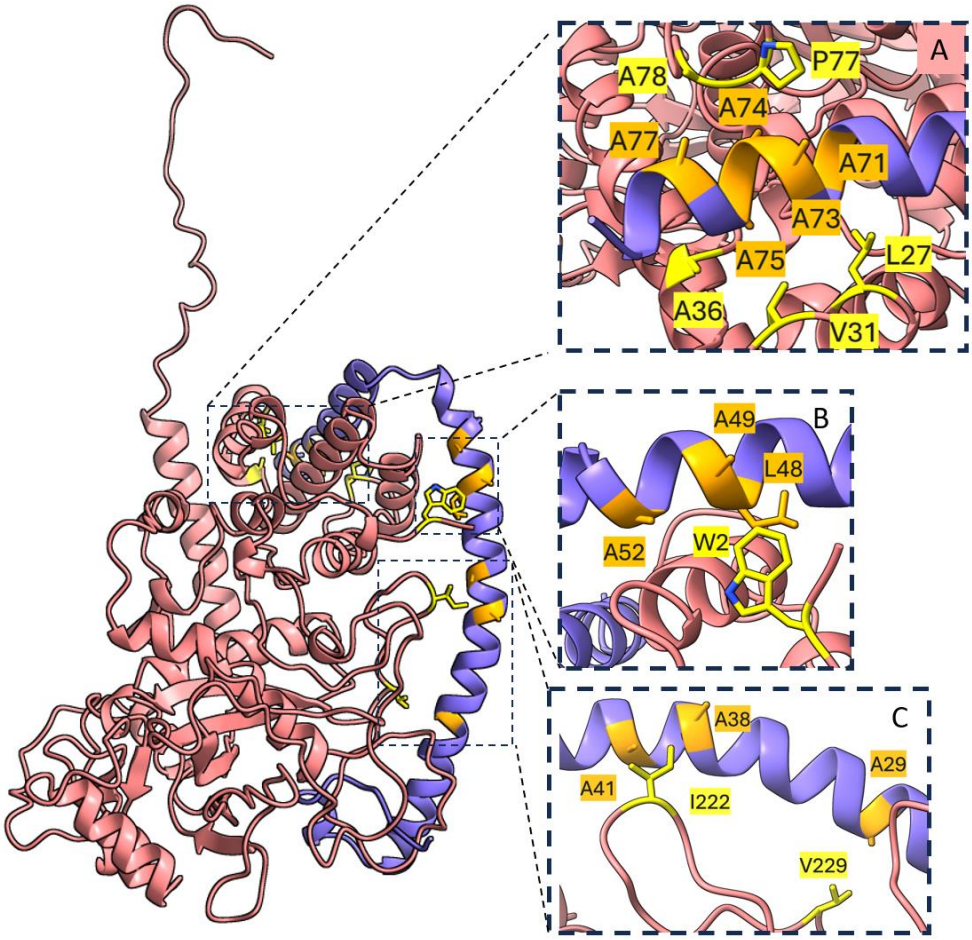

Figure 11 The predicted structure of UL12.5 as a cartoon model (pink) together with binder #766 (purple), with highlighted atoms of residues A71, A73, A74, A77, L48, A49, A42, A29, A39, A41 (orange) and L27, P77, A78, W2, V229, I222 (yellow) to show potential hydrophobic interactions, visualised using ChimeraX

The potential hydrophobic interactions between binder #766 and UL12.5 can be seen in figure 11. Figure 11A shows the possible hydrophobic interactions of the alpha helix that aligns with the top of the UL12.5. The residues alanine ($A71_{binder}$) with leucine ($L27_{UL12.5}$), two alanine residues ($A73_{binder}$ and $A75_{binder}$) with proline ($P77_{binder}$) and alanine ($A71_{binder}$) with alanine ($A78_{UL12.5}$) are poised to interact in this region. The tryptophan residue ($W2_{UL12.5}$) which is orientated towards the long alpha helix on the binder has potential interactions with the residues alanine ($A49_{binder}$), alanine ($A52_{binder}$) and leucine ($L48_{binder}$) on the binder, as shown in figure 11B. Furthermore, in figure 11C potential hydrophobic interactions between two alanine residues ($A38_{binder}$ and $A41_{binder}$) with isoleucine ($I222_{UL12.5}$) and between another alanine ($A29_{binder}$) and valine ($V229_{UL12.5}$) are depicted. The proximity of the interacting residues can be seen in table 2.

Table 2 List of residues on binder #766 and UL12.5 predicted to engage in hydrophobic interactions, with the measured distance between the corresponding pairs

Residues with potential hydrophobic interaction between binder #766 and UL12.5	**Distance**
$A71_{binder}$-$L27_{UL12.5}$	4.478 Å
$A73_{binder}$-$P77_{UL12.5}$	3.931 Å
$A74_{binder}$-$P77_{UL12.5}$	3.977 Å
$A77_{binder}$-$A78_{UL12.5}$	3.746 Å
$L48_{binder}$-$W2_{UL12.5}$	3.550 Å
$A49_{binder}$-$W2_{UL12.5}$	4.098 Å
$A52_{binder}$-$W2_{UL12.5}$	4.982 Å
$A29_{binder}$-$V229_{UL12.5}$	3.952 Å
$A38_{binder}$-$I222_{UL12.5}$	3.962 Å
$A41_{binder}$-$W2_{UL12.5}$	4.652 Å

Figure 12 shows the predicted structure of binder #136 (purple), which has a helix-helix-sheet structure when looking from the N- to the C-terminus, together with the predicted structure of UL12.5 (pink). The binder consist of 118 amino acids covering a large area of UL12.5 around the N-terminus.

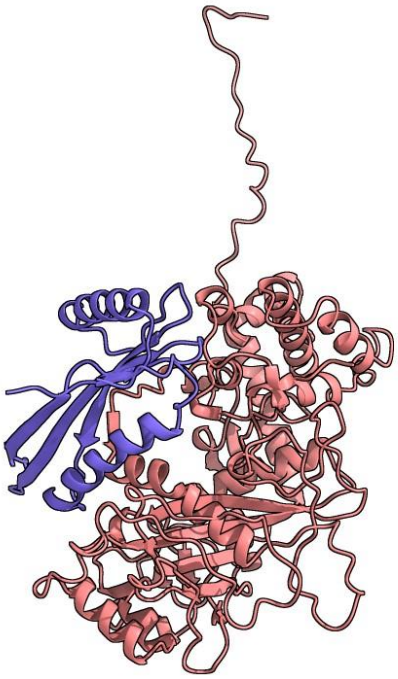

Figure 12 The predicted structure of UL12.5 as a cartoon model (pink) together with binder #136 (purple), visualised using ChimeraX

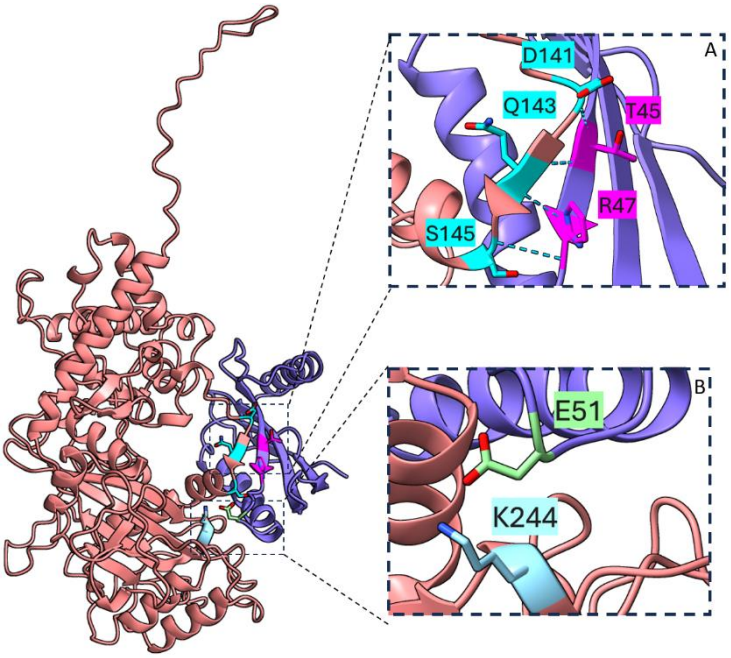

Figure 13 The predicted structure of UL12.5 as a cartoon model (pink) together with binder #136 (purple), visualised using ChimeraX (A) highlights atoms of residues T45, T47 (magenta) and D141, Q143, S145 (cyan)to show potential hydrogen bond (dashed blue line) (B) highlights atoms of residues E51 (green) and K244 (blue) to show potential electrostatic interactions

Figure 13A illustrates the potential hydrogen bonds between binder #136 and UL12.5. There is a possible hydrogen bond between aspartic acid ($D141_{UL12.5)}$ and threonine ($T45_{binder}$), with a distance of 1.815 Å. Glutamine ($Q143_{UL12.5}$) can engage in a hydrogen bond with both threonine ($T45_{binder}$) and arginine ($R47_{binder}$), at a distance of 1.859 Å and 2.255 Å respectively. Additionally, a hydrogen bond can be formed between serine ($S145_{UL12.5}$) and arginine ($R47_{binder}$) positioned 2.293 Å away from each other.

Moreover, there is one potential electrostatic interaction between the residues lysine ($K244_{UL12.5}$) and glutamic acid ($E51_{binder}$), which are approximately 3.264 Å away from each other, as illustrated in figure 13B.

Potential hydrophobic interactions between binder #136 and UL12.5 can be seen in figure 14. There are three potential interactions, the first one being between valine ($V40_{binder}$) and alanine ($A10_{UL12.5}$), the second between isoleucine ($I44_{binder}$) and proline ($P140_{UL12.5}$) and the last between alanine ($A63_{binder}$) and valine ($V152_{UL12.5}$). The proximity of the interacting residues can be seen in table 3.

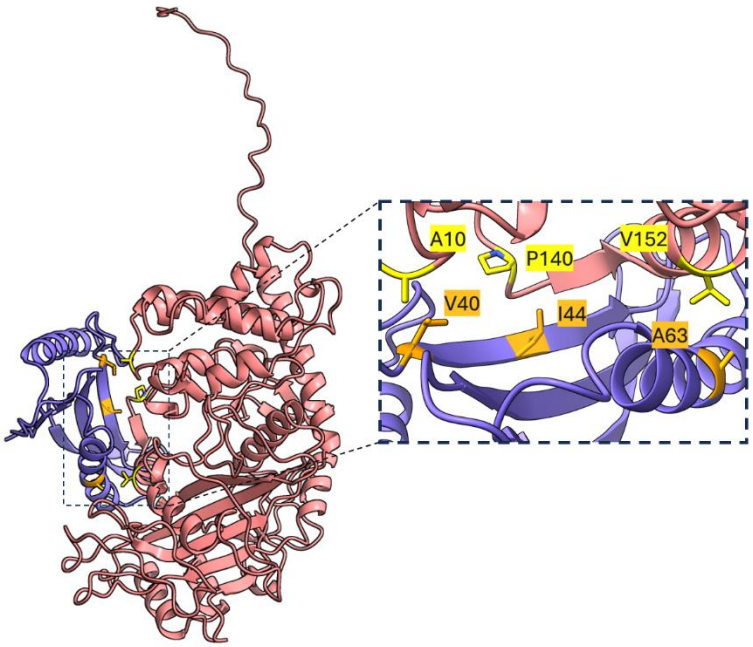

Figure 14 The predicted structure of UL12.5 as a cartoon model (pink) together with binder #136 (purple), with highlighted atoms of residues V40, I44, A63 (orange) and A10, P140,V152 (yellow) to show potential hydrophobic interactions, visualised using ChimeraX

Table 3 List of residues on binder #136 and UL12.5 predicted to engage in hydrophobic interactions, with the measured distance between the corresponding pairs

Residues with potential hydrophobic interaction between binder #878 and UL12.5	**Distance**
$A40_{binder}$-$A10_{UL12.5}$	3.744 Å
$I44_{binder}$-$P140_{UL12.5}$	4.114 Å
$A63_{binder}$-$V152_{UL12.5}$	4.826 Å

DISCUSSION

Using the computational *de novo* protein design pipeline a total of 1500 protein binders were designed against UL12.5. None of the designed protein binders were given a pAE interaction score below the cut-off value of 10, below which according to literature the success rate of correctly predicted binders significantly increases [16]. Consequently, none of the designed binders were identified to be high-affinity binders targeting the viral UL12.5 protein. Nonetheless, the three best designed binders were analysed. The structure of these binders consists mainly of alpha helices, with binder #136 also containing a beta-sheet. This is since RFdiffusion favours alpha helices, beta-sheets or mixed topologies, as these structures are stable [11].

When looking at the structures of the binders, it is noticeable that binder #878 is a small rigid molecule consisting of a few alpha helices. This smaller stable structure likely contributes to a lower interaction score in comparison to binders #766 and #136, which are larger and less globular, causing them to be less stable.

When focusing on possible interactions between the binders and UL12.5, this revealed that there are some potential hydrogen bonds and electrostatic and hydrophobic interactions.

Firstly, all three binders seem to engage in hydrophobic interactions. Binder #878 and binder #136 have only three possible hydrophobic interactions, which do not contribute much to the binding affinity against UL12.5. Binder #766 seems to engage in ten possible interactions. However, during investigation of possible hydrophobic interactions it was apparent that besides the residues towards the binding interface, the long stretched alpha helix also contains an abundance of hydrophobic residues on the side facing a potential solvent (figure 15). If this binder were to be used in solution, in general buried hydrophobic residues would be energetically more favourable. Therefore, the presence of the long alpha-helix as predicted may be structurally unfavourable, potentially resulting in the binder folding into a different conformation than predicted.

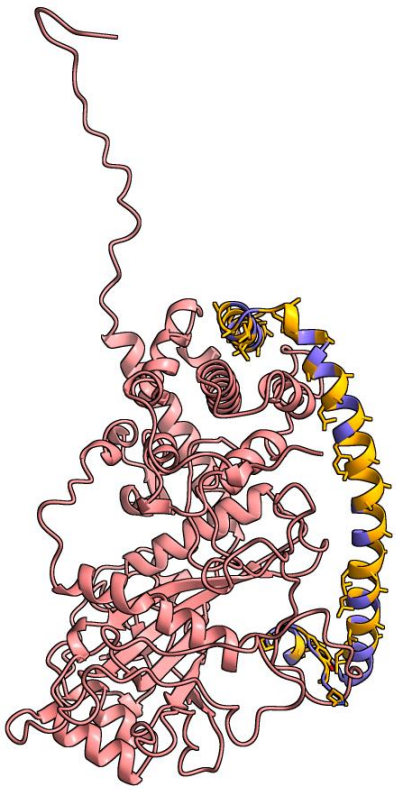

Figure 15 The predicted structure of UL12.5 as a cartoon model (pink) together with binder #766 (purple), with highlighted hydrophobic residues (orange), visualised using ChimeraX

Moreover, there were a few potential hydrogen bonds found on both binder #766 and #136. However, binder #766 has only one potential hydrogen bond while on binder #136 only two different residues can engage in hydrogen bonds, therefore the hydrogen bonds also do not seem to have a major impact of the binding affinity.

In addition, potential electrostatic interactions between binder #766 and UL12.5 were observed, as illustrated in figure 10. That being said, the orientation of these residues is not optimal since interacting residues are directed away from each other. A limitation of AF2 is that the program creates a static snapshot of a possible protein configuration, while in the cell proteins can change their configuration as protein are dynamic, allowing residues to orientate in a more favourable direction and therefore form stronger interactions [15]. On the contrary, the electrostatic interaction on binder #136 is orientated in a favourable direction. However, since there is only one possible interaction it does not have a significant effect on the binding affinity. Nonetheless, since these binders have an interaction score above 10 they are unlikely to have a successful configuration. Consequently the interaction found are not expected to occur *in vitro*.

It can be concluded that the low number of interactions in combination with the fact that the potential interactions found are not optimal, resulted in a higher interaction score and low-affinity binders.

Upon further analysis of electrostatic interactions, UL12.5 was found to have an abundance of positively charged residues, while the designed binders predominantly featured negatively charged residues. This aligns with UL12.5's role as a DNase, which typically binds to negatively charged DNA.

Consequently, UL12.5 is naturally more polar (figure 16) and there are fewer hydrophobic pockets capable of forming hydrophobic interactions, which have an important role during protein folding [18]. This makes it challenging to design successful high-affinity protein binders against UL12.5.

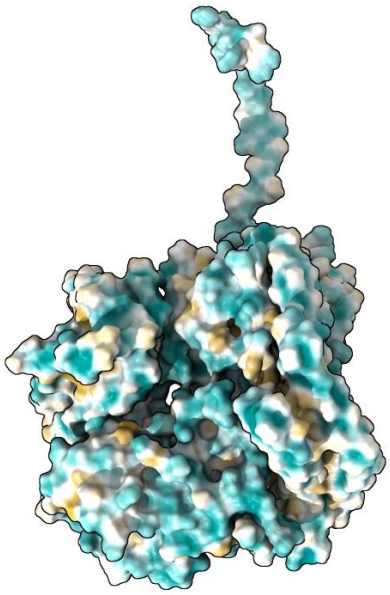

Figure 16 The predicted hydrophobic potential surface of UL12.5, visualised using ChimeraX

Future studies are required to predict binding spots which have a crucial role inhibiting UL12.5's activity. Additionally, hotspots, which are residues that play an essential role in the protein or protein-protein interactions can be incorporated as target sites for the new binders. Generally, hotspots are hydrophobic residues on the target since in comparison to salt-bridges or hydrogen bonds, these interactions are stronger. In order to design protein binders which would inhibit UL12.5 in a competitive manner, these hotspots would be located in the active site, which is in the centre of UL12.5. However, as previously mentioned, UL12.5 binds to DNA. Therefore, targeting the active site directly might be challenging due to its polarity. An alternative and potentially more effective approach could be to target an external site on the protein, to design a protein binder that allosterically inhibits UL12.5. If this results in binders with a pAE interaction score below 10, these high-affinity binders can be analysed further during *in vitro* and *in cellulo* experiments. Notably, in order to be successful *in cellulo* according to literature an interaction score below 5 is desired [11]. If these experiments demonstrate that the designed binders reduce mtDNA degradation and reactivation of latent reservoirs, the binders can be used to develop a novel therapeutic against HSV-1.

CONCLUSION

In this research project a *de novo* protein pipeline —using a computational approach— was used to generate protein binders targeting the HSV-1 protein UL12.5, with the goal of designing high-affinity binders. Unfortunately, none of the predicted protein binders demonstrate high-affinity interactions with UL12.5 (all binders have interaction score above 10). The number of interactions was insufficient, and most of the identified interactions were suboptimal in terms of distance and orientation, which explains the low binding affinity for the UL12.5 protein. Additionally, since the confidence of the prediction being folded in the correct conformation is above the cut-off value it is unlikely for these interactions to occur *in vitro*. Future studies could improve the design strategy by biasing the binders toward specific hotspots critical for UL12.5's activity. If this approach yields high-affinity binders, these candidates can be tested *in vitro* and *in cellulo* to analyse their ability to inhibit UL12.5's activity. Successful binders could prevent HSV-1 reactivation and limit mitochondrial damage, contributing to the development of a novel therapeutic that would be particularly beneficial for immunocompromised patients.

REFERENCES

1. Arduino, P. G., & Porter, S. R. (2007). Herpes Simplex Virus Type 1 infection: overview on relevant clinico-pathological features*. *Journal of Oral Pathology & Medicine*, *37*(2), 107–121. https://doi.org/10.1111/j.1600-0714.2007.00586.x

2. Su, D., Han, L., Shi, C., Li, Y., Qian, S., Feng, Z., & Yu, L. (2024). An updated review of HSV-1 infection-associated diseases and treatment, vaccine development, and vector therapy application. *Virulence*, *15*(1). https://doi.org/10.1080/21505594.2024.2425744

3. Booy, F. P., Newcomb, W. W., Trus, B. L., Brown, J. S., Baker, T. B., & Steven, A. C. (1991). Liquid-crystalline, phage-like packing of encapsidated DNA in herpes simplex virus. *Cell*, *64*(5), 1007–1015. https://doi.org/10.1016/0092-8674(91)90324-r

4. Suzich, J. B., & Cliffe, A. R. (2018). Strength in diversity: Understanding the pathways to herpes simplex virus reactivation. *Virology*, *522*(0042-6822), 81–91. https://doi.org/10.1016/j.virol.2018.07.011

5. Krakowiak, P. A., Flores, M. E., Cuddy, S. R., Whitford, A. L., Dochnal, S. A., Babnis, A., Miyake, T., Tigano, M., Engel, D. A., & Cliffe, A. R. (2025). Co-option of mitochondrial nucleic acid–sensing pathways by HSV-1 UL12.5 for reactivation from latent infection. *Proceedings of the National Academy of Sciences*, *122*(4). https://doi.org/10.1073/pnas.2413965122

6. Corcoran, J. A., Saffran, H. A., Duguay, B. A., & Smiley, J. R. (2009). Herpes Simplex Virus UL12.5 Targets Mitochondria through a Mitochondrial Localization Sequence Proximal to the N Terminus. *Journal of Virology*, *83*(6), 2601–2610. https://doi.org/10.1128/jvi.02087-08

7. West, A. P., Shadel, G. S., & Ghosh, S. (2011). Mitochondria in innate immune responses. *Nature Reviews Immunology*, *11*(6), 389–402. https://doi.org/10.1038/nri2975

8. Van den Broek M. (2024). Purification and characterisation of Herpes Simplex Virus 1 DNase UL12.5 as a potential target for prevention of Alzheimer's Disease. MSc Research Project Molecular Pharmacology, UMCG (provided by K. Rafie)

9. Sadowski, L. A., Upadhyay, R., Greeley, Z. W., & Margulies, B. J. (2021). Current Drugs to Treat Infections with Herpes Simplex Viruses-1 and -2. *Viruses*, *13*(7), 1228. https://doi.org/10.3390/v13071228

10. Sharma, D., Sharma, S., Akojwar, N., Dondulkar, A., Yenorkar, N., Pandita, D., Prasad, S. K., & Dhobi, M. (2023). An Insight into Current Treatment Strategies, Their Limitations, and Ongoing Developments in Vaccine Technologies against Herpes Simplex Infections. *Vaccines*, *11*(2), 206. https://doi.org/10.3390/vaccines11020206

11. Watson, J. L., Juergens, D., Bennett, N. R., Trippe, B. L., Yim, J., Eisenach, H. E., Ahern, W., Borst, A. J., Ragotte, R. J., Milles, L. F., Wicky, B. I. M., Hanikel, N., Pellock, S. J., Courbet, A., Sheffler, W., Wang, J., Venkatesh, P., Sappington, I., Torres, S. V., & Lauko, A. (2023). De novo design of protein structure and function with RFdiffusion. *Nature*, *620*, 1089–1100. https://doi.org/10.1038/s41586-023-06415-8

12. Dauparas, J., Anishchenko, I., Bennett, N., Bai, H., Ragotte, R. J., Milles, L. F., Wicky, B. I. M., Courbet, A., de Haas, R. J., Bethel, N., Leung, P. J. Y., Huddy, T. F., Pellock, S., Tischer, D., Chan, F., Koepnick, B., Nguyen, H., Kang, A., Sankaran, B., & Bera, A. K. (2022). Robust deep learning–based protein sequence design using ProteinMPNN. *Science*, *378*(6615), 49–56. https://doi.org/10.1126/science.add2187

13. Jumper, J., Evans, R., Pritzel, A., Green, T., Figurnov, M., Ronneberger, O., Tunyasuvunakool, K., Bates, R., Žídek, A., Potapenko, A., Bridgland, A., Meyer, C., Kohl, S. A. A., Ballard, A. J., Cowie, A., Romera-Paredes, B., Nikolov, S., Jain, R., Adler, J., & Back, T. (2021). Highly Accurate Protein Structure Prediction with Alphafold. *Nature*, *596*(7873), 583–589. https://doi.org/10.1038/s41586-021-03819-2

14. EMBL-EBI. (n.d.). *PAE: A measure of global confidence in AlphaFold2 predictions | AlphaFold*. EMBL-EBI. https://www.ebi.ac.uk/training/online/courses/alphafold/inputs-and-outputs/evaluating-alphafolds-predicted-structures-using-confidence-scores/pae-a-measure-of-global-confidence-in-alphafold-predictions/

15. Guo, H.-B., Perminov, A., Bekele, S., Kedziora, G., Farajollahi, S., Varaljay, V., Hinkle, K., Molinero, V., Meister, K., Hung, C., Dennis, P., Kelley-Loughnane, N., & Berry, R. (2022). AlphaFold2 models indicate that protein sequence determines both structure and dynamics. *Scientific Reports*, *12*(1), 10696. https://doi.org/10.1038/s41598-022-14382-9

16. Bennett, N., Coventry, B., Inna Goreshnik, Huang, B., Allen, A., Vafeados, D., Ying Po Peng, Justas Dauparas, Baek, M., Stewart, L., DiMaio, F., Steven De Munck, Savvides, S. N., & Baker, D. (2023). Improving *de novo* protein binder design with deep learning. *Nature Communications*, *14*(1), 2625–2625. https://doi.org/10.1038/s41467-023-38328-5

17. Meng, E. C., Goddard, T. D., Pettersen, E. F., Couch, G. S., Pearson, Z. J., Morris, J. H., & Ferrin, T. E. (2023). UCSF ChimeraX: Tools for Structure Building and Analysis. *Protein Science: A Publication of the Protein Society*, *32*(11), e4792. https://doi.org/10.1002/pro.4792

18. Camilloni, C., Bonetti, D., Morrone, A., Giri, R., Dobson, C. M., Brunori, M., Gianni, S., & Vendruscolo, M. (2016). Towards a structural biology of the hydrophobic effect in protein folding. *Scientific Reports*, *6*(1), 28285. https://doi.org/10.1038/srep28285

Appendix

The raw data of pAE interaction scores for the designed binders, as calculated by AF2, are presented in Figures 17 to 22.

binder number	pae_interaction	binder number	pae_interaction	binder number	pae_interaction	binder number	pae_interaction	binder number	pae_interaction	binder number	pae_interaction	binder number	pae_interaction	binder number	pae_interaction	binder number	pae_interaction
1	28,23	31	27,948	61	28,369	91	28,429	121	28,158	151	27,78	181	28,386	211	28,157	241	28,491
2	28,301	32	28,04	62	28,066	92	27,998	122	27,623	152	28,431	182	28,205	212	27,981	242	28,319
3	28,43	33	28,282	63	28,229	93	19,705	123	27,999	153	28,116	183	28,397	213	28,211	243	28,391
4	28,4	34	27,848	64	27,736	94	24,169	124	28,064	154	25,598	184	27,752	214	28,224	244	27,658
5	28,512	35	28,095	65	28,005	95	27,896	125	28,12	155	28,116	185	26,132	215	28,084	245	28,017
6	28,22	36	28,134	66	28,396	96	27,707	126	28,164	156	28,258	186	28,253	216	28,087	246	27,286
7	28,207	37	28,054	67	28,383	97	27,978	127	28,405	157	28,166	187	28,282	217	27,506	247	28,202
8	28,042	38	27,972	68	28,222	98	27,881	128	28,734	158	28,536	188	28,246	218	28,453	248	28,148
9	28,181	39	28,186	69	28,003	99	27,324	129	27,828	159	28,241	189	27,434	219	27,997	249	28,105
10	27,848	40	28,211	70	28,224	100	27,738	130	27,831	160	28,338	190	28,303	220	28,14	250	28,388
11	27,666	41	28,115	71	28,284	101	28,494	131	28,409	161	28,066	191	27,77	221	28,197	251	27,993
12	28,135	42	28,135	72	27,504	102	28,449	132	28,212	162	28,161	192	28,054	222	27,165	252	27,943
13	28,228	43	28,3	73	28,086	103	28,238	133	28,172	163	28,159	193	28,123	223	28,402	253	28,023
14	24,017	44	28,334	74	28,353	104	28,133	134	28,129	164	28,436	194	27,264	224	24,583	254	28,229
15	27,865	45	28,297	75	28,573	105	28,274	135	28	165	28,28	195	28,096	225	28,053	255	27,731
16	27,941	46	27,94	76	28,061	106	28,04	136	16,682	166	28,288	196	28,37	226	27,769	256	28,029
17	28,269	47	28,068	77	28,431	107	28,302	137	28,045	167	28,371	197	28,408	227	27,815	257	28,107
18	28,212	48	28,25	78	28,26	108	28,141	138	28,41	168	28,424	198	28,254	228	28,233	258	28,122
19	27,845	49	28,25	79	28,533	109	28,196	139	27,99	169	28,213	199	28,05	229	27,985	259	28,321
20	28,165	50	28,309	80	28,247	110	28,266	140	28,015	170	27,564	200	28,358	230	28,114	260	28,314
21	28,35	51	27,845	81	28,158	111	28,178	141	28,247	171	28,41	201	27,827	231	27,812	261	28,413
22	28,189	52	28,536	82	28,408	112	19,068	142	28,22	172	28,433	202	27,757	232	28,272	262	20,197
23	28,371	53	28,421	83	28,524	113	27,441	143	25,241	173	28,169	203	28,514	233	28,246	263	28,374
24	27,931	54	19,898	84	28,18	114	28,142	144	28,063	174	28,34	204	18,234	234	27,511	264	28,109
25	28,016	55	27,943	85	28,378	115	28,273	145	28,218	175	28,534	205	27,943	235	28,021	265	28,435
26	28,142	56	28,297	86	28,196	116	28,242	146	28,173	176	27,791	206	28,235	236	27,229	266	28,375
27	28,284	57	28,157	87	27,67	117	28,393	147	28,373	177	28,027	207	28,532	237	27,749	267	27,553
28	28,519	58	28,369	88	28,106	118	27,874	148	27,97	178	28,209	208	28,497	238	27,775	268	28,048
29	28,374	59	28,052	89	28,09	119	28,254	149	28,419	179	28,503	209	27,895	239	28,074	269	28,486
30	28,128	60	28,101	90	28,231	120	28,105	150	27,645	180	28,154	210	28,161	240	28,347	270	28,208

Figure 17 Raw data of the designed protein binders 1 up until 270 with their pAE interaction score, scored using AF2.

binder number	pae_interaction	binder number	pae_interaction	binder number	pae_interaction	binder number	pae_interaction	binder number	pae_interaction	binder number	pae_interaction	binder number	pae_interaction	binder number	pae_interaction	binder number	pae_interaction
271	28,15	301	28,261	331	28,362	361	28,203	391	28,051	421	28,313	451	28,296	481	28,283	511	28,373
272	27,834	302	28,298	332	28,31	362	28,293	392	28,239	422	27,994	452	28,288	482	28,171	512	28,206
273	28,203	303	28,223	333	28,193	363	28,47	393	28,145	423	20,481	453	28,442	483	28,127	513	28,4
274	28,265	304	27,834	334	28,2	364	28,343	394	28,049	424	28,216	454	28,235	484	18,632	514	28,441
275	28,154	305	28,262	335	27,473	365	28,23	395	27,735	425	28,388	455	28,341	485	28,186	515	28,473
276	28,104	306	28,452	336	28,096	366	28,353	396	28,174	426	27,895	456	26,964	486	27,993	516	28,296
277	28,534	307	28,476	337	28,378	367	27,886	397	28,206	427	28,208	457	28,486	487	28,352	517	27,998
278	27,978	308	28,037	338	28,08	368	25,92	398	28,109	428	27,969	458	27,566	488	28,297	518	28,298
279	28,357	309	28,092	339	27,966	369	28,433	399	28,159	429	28,103	459	24,119	489	28,287	519	28,334
280	28,287	310	28,49	340	27,645	370	28,237	400	28,331	430	28,336	460	28,285	490	28,287	520	27,835
281	28,345	311	28,006	341	26,997	371	28,38	401	28,235	431	28,396	461	28,088	491	27,833	521	27,567
282	28,41	312	27,842	342	28,14	372	27,784	402	28,317	432	27,959	462	28,686	492	28	522	28,222
283	28,216	313	28,162	343	28,116	373	28,229	403	28,164	433	28,262	463	28,265	493	27,593	523	28,223
284	28,247	314	28,087	344	27,886	374	28,371	404	28,678	434	28,029	464	28,243	494	28,108	524	28,347
285	28,478	315	28,168	345	28,494	375	28,292	405	27,87	435	27,971	465	28,644	495	28,268	525	28,512
286	28,133	316	28,121	346	28,105	376	28,265	406	28,371	436	28,221	466	28,233	496	28,07	526	28,017
287	28,39	317	28,404	347	28,103	377	28,38	407	28,358	437	27,463	467	28,08	497	28,044	527	28,149
288	28,355	318	27,916	348	28,251	378	28,026	408	28,182	438	28,28	468	27,846	498	28,402	528	28,128
289	28,11	319	28,359	349	28,119	379	28,19	409	28,138	439	28,389	469	28,333	499	28,14	529	28,269
290	28,446	320	28,191	350	28,537	380	28,136	410	28,193	440	28,09	470	28,087	500	28,051	530	28,266
291	28,14	321	28,435	351	28,415	381	28,414	411	27,978	441	27,819	471	28,24	501	28,193	531	28,363
292	26,934	322	28,435	352	28,369	382	27,836	412	28,39	442	28,285	472	28,267	502	28,383	532	28,611
293	28,167	323	27,794	353	28,148	383	28,597	413	28,356	443	28,044	473	28,032	503	28,1	533	28,448
294	28,135	324	28,37	354	28,119	384	26,94	414	28,204	444	28,233	474	28,285	504	28,14	534	28,382
295	27,66	325	28,371	355	28,336	385	27,638	415	28,253	445	28,166	475	28,268	505	28,011	535	28,324
296	28,125	326	27,871	356	28,34	386	28,231	416	28,04	446	28,443	476	28,142	506	28,071	536	28,234
297	28,142	327	28,127	357	28,301	387	28,422	417	24,722	447	28,41	477	28,013	507	27,791	537	27,26
298	28,566	328	28,036	358	28,004	388	27,741	418	27,897	448	27,244	478	28,216	508	28,343	538	28,41
299	28,123	329	28,429	359	28,18	389	28,234	419	28,286	449	28,428	479	28,091	509	28,08	539	28,025
300	28,423	330	28,359	360	28,398	390	28,273	420	27,798	450	28,254	480	25,837	510	28,451	540	28,2

Figure 18 Raw data of the designed protein binders 271 up until 540 with their pAE interaction score, scored using AF2.

binder number	pae_interaction	binder number	pae_interaction	binder number	pae_interaction	binder number	pae_interaction	binder number	pae_interaction	binder number	pae_interaction	binder number	pae_interaction	binder number	pae_interaction	binder number	pae_interaction
541	28,658	571	28,337	601	27,936	631	28,021	661	28,423	691	27,855	721	28,186	751	28,075	781	28,5
542	27,886	572	28,435	602	28,021	632	27,818	662	28,145	692	28,434	722	28,073	752	28,448	782	27,973
543	28,164	573	28,216	603	28,397	633	28,322	663	27,313	693	28,372	723	27,866	753	28,51	783	28,274
544	28,087	574	27,142	604	27,909	634	28,374	664	28,151	694	28,249	724	28,04	754	28,082	784	28,372
545	28,12	575	28,306	605	28,234	635	27,735	665	28,136	695	27,935	725	28,329	755	27,978	785	28,558
546	28,145	576	28,399	606	28,709	636	28,134	666	27,926	696	28,264	726	28,276	756	28,417	786	27,929
547	27,915	577	27,869	607	28,177	637	27,85	667	28,116	697	27,783	727	28,229	757	28,354	787	28,31
548	27,281	578	28,383	608	28,425	638	28,368	668	28,156	698	28,374	728	27,862	758	28,048	788	28,189
549	28,235	579	28	609	27,874	639	27,9	669	28,053	699	28,029	729	28,31	759	27,084	789	28,103
550	28,192	580	28,555	610	28,202	640	28,441	670	27,633	700	27,942	730	28,318	760	28,309	790	27,46
551	28,136	581	28,089	611	28,065	641	25,363	671	27,939	701	28,475	731	27,888	761	28,557	791	28,271
552	28,003	582	28,175	612	28,376	642	28,513	672	23,883	702	28,397	732	28,309	762	27,43	792	28,161
553	28,377	583	28,101	613	28,213	643	28,253	673	27,813	703	27,959	733	28,366	763	27,123	793	28,396
554	28,024	584	28,496	614	22,143	644	28,081	674	28,022	704	28,278	734	27,975	764	28,183	794	27,93
555	27,846	585	28,102	615	28,408	645	28,19	675	28,545	705	28,127	735	28,204	765	28,111	795	28,467
556	28,239	586	28,107	616	28,242	646	28,22	676	28,533	706	25,376	736	27,856	766	15,763	796	28,084
557	28,053	587	25,977	617	28,134	647	28,25	677	28,006	707	28,542	737	27,748	767	27,742	797	28,047
558	27,66	588	27,902	618	27,245	648	28,42	678	27,823	708	28,283	738	28,136	768	28,339	798	27,978
559	28,256	589	27,883	619	28,418	649	27,21	679	28,466	709	26,924	739	28,292	769	28,371	799	28,215
560	28,202	590	28,051	620	28,282	650	28,297	680	28,541	710	28,077	740	28,11	770	28,17	800	28,063
561	28,36	591	28,24	621	28,245	651	28,499	681	28,286	711	28,089	741	28,091	771	28,37	801	28,403
562	27,984	592	28,454	622	27,985	652	27,779	682	28,391	712	27,849	742	28,382	772	27,817	802	28,206
563	24,416	593	28,376	623	28,507	653	28,049	683	28,389	713	28,291	743	28,19	773	28,225	803	28,217
564	28,415	594	28,055	624	28,204	654	28,452	684	27,793	714	28,314	744	28,214	774	27,874	804	28,235
565	28,116	595	28,121	625	28,581	655	28,273	685	27,776	715	18,041	745	25,506	775	28,028	805	28,568
566	28,054	596	28,243	626	25,136	656	28,053	686	28,29	716	28,462	746	28,052	776	28,24	806	27,858
567	27,831	597	18,806	627	28,262	657	27,887	687	28,147	717	28,315	747	28,311	777	27,886	807	28,204
568	28,017	598	28,087	628	27,913	658	28,328	688	27,64	718	28,21	748	28,492	778	28,124	808	28,078
569	22,445	599	28,27	629	28,404	659	28,294	689	28,331	719	28,037	749	28,015	779	28,367	809	28,284
570	28,197	600	27,715	630	28,246	660	28,139	690	28,36	720	28,213	750	28,132	780	28,338	810	28,129

Figure 19 Raw data of the designed protein binders 541 up until 810 with their pAE interaction score, scored using AF2.

binder number	pae_interaction	binder number	pae_interaction	binder number	pae_interaction	binder number	pae_interaction	binder number	pae_interaction	binder number	pae_interaction	binder number	pae_interaction	binder number	pae_interaction	binder number	pae_interaction
811	28,081	841	27,732	871	28,111	901	27,799	931	27,506	961	28,318	991	28,086	1021	28,24	1021	28,24
812	27,845	842	27,643	872	28,21	902	28,047	932	28,405	962	28,335	992	27,43	1022	28,405	1022	28,405
813	27,944	843	27,939	873	28,142	903	28,055	933	28,28	963	27,698	993	27,905	1023	28,298	1023	28,298
814	27,98	844	28,083	874	27,491	904	27,977	934	28,153	964	27,672	994	27,746	1024	28,453	1024	28,453
815	28,309	845	28,018	875	28,504	905	28,187	935	28,327	965	28,185	995	27,737	1025	28,369	1025	28,369
816	28,135	846	27,139	876	28,324	906	28,271	936	28,326	966	26,854	996	28,312	1026	28,246	1026	28,246
817	28,387	847	28,038	877	28,423	907	28,246	937	28,22	967	28,01	997	28,302	1027	28,311	1027	28,311
818	28,134	848	28,305	878	14,042	908	28,234	938	28,289	968	28,345	998	28,171	1028	28,09	1028	28,09
819	27,907	849	28,177	879	27,951	909	28,254	939	28,171	969	28,269	999	28,412	1029	28,278	1029	28,278
820	27,853	850	28,19	880	28,193	910	28,242	940	28,273	970	27,712	1000	27,735	1030	28,245	1030	28,245
821	28,245	851	28,334	881	28,203	911	28,236	941	28,25	971	28,146	1001	28,535	1031	28,044	1031	28,044
822	28,019	852	28,003	882	28,058	912	28,133	942	28,171	972	27,804	1002	28,223	1032	28,321	1032	28,321
823	28,078	853	28,461	883	18,58	913	27,992	943	28,402	973	28,305	1003	27,324	1033	28,393	1033	28,393
824	28,013	854	28,357	884	28,396	914	28,232	944	28,157	974	28,239	1004	28,056	1034	28,249	1034	28,249
825	28,363	855	28,245	885	28,381	915	28,259	945	28,329	975	28,356	1005	28,217	1035	28,096	1035	28,096
826	28,112	856	28,009	886	28,467	916	28,425	946	28,272	976	28,024	1006	28,09	1036	28,364	1036	28,364
827	28,441	857	28,166	887	28,18	917	27,949	947	28,046	977	28,153	1007	28,375	1037	28,248	1037	28,248
828	28,202	858	27,873	888	28,234	918	28,688	948	28,457	978	28,388	1008	28,554	1038	28,338	1038	28,338
829	28,239	859	28,231	889	28,148	919	28,16	949	27,964	979	28,267	1009	19,943	1039	28,058	1039	28,058
830	27,96	860	28,103	890	28,082	920	28,383	950	23,866	980	28,263	1010	28,351	1040	28,283	1040	28,283
831	28,228	861	28,128	891	28,216	921	28,255	951	27,999	981	28,26	1011	27,899	1041	27,987	1041	27,987
832	28,424	862	27,958	892	28,371	922	28,385	952	28,173	982	28,31	1012	28,072	1042	28,594	1042	28,594
833	28,056	863	27,242	893	28,431	923	28,515	953	27,779	983	27,866	1013	28,263	1043	28,016	1043	28,016
834	28,259	864	27,872	894	25,486	924	28,172	954	27,945	984	28,465	1014	28,013	1044	28,264	1044	28,264
835	28,159	865	27,895	895	28,169	925	28,198	955	27,287	985	28,372	1015	28,188	1045	28,122	1045	28,122
836	27,954	866	28,148	896	28,462	926	28,212	956	28,235	986	27,944	1016	26,853	1046	28,312	1046	28,312
837	28,24	867	27,943	897	28,096	927	28,27	957	28,187	987	28,355	1017	27,858	1047	28,217	1047	28,217
838	28,077	868	28,362	898	28,215	928	28,289	958	21,597	988	28,028	1018	28,419	1048	28,384	1048	28,384
839	25,398	869	27,861	899	27,984	929	27,913	959	28,029	989	28,365	1019	28,316	1049	27,913	1049	27,913
840	28,026	870	27,774	900	28,226	930	28,358	960	28,155	990	28,365	1020	27,188	1050	28,156	1050	28,156

Figure 20 Raw data of the designed protein binders 811 up until 1050 with their pAE interaction score, scored using AF2.

binder number	pae_interaction	binder number	pae_interaction	binder number	pae_interaction	binder number	pae_interaction	binder number	pae_interaction	binder number	pae_interaction	binder number	pae_interaction	binder number	pae_interaction	binder number	pae_interaction
1081	28,177	1111	28,199	1141	28,226	1171	28,306	1201	27,673	1231	28,244	1261	28,152	1291	26,442	1321	27,94
1082	27,798	1112	28,545	1142	28,524	1172	28,406	1202	28,381	1232	28,027	1262	27,948	1292	28,182	1322	28,25
1083	28,046	1113	28,06	1143	28,331	1173	27,981	1203	28,229	1233	28,075	1263	28,383	1293	28,122	1323	28,407
1084	28,123	1114	28,011	1144	27,769	1174	28,257	1204	28,314	1234	28,108	1264	21,655	1294	28,308	1324	28,219
1085	28,244	1115	28,133	1145	28,124	1175	27,97	1205	28,478	1235	26,822	1265	28,364	1295	28,508	1325	28,285
1086	27,836	1116	27,304	1146	28,225	1176	28,216	1206	28,122	1236	28,105	1266	27,943	1296	28,393	1326	28,411
1087	27,885	1117	28,355	1147	28,139	1177	28,039	1207	28,169	1237	28,587	1267	28,143	1297	28,579	1327	28,142
1088	28,128	1118	27,909	1148	28,412	1178	28,294	1208	28,279	1238	28,194	1268	27,902	1298	27,149	1328	27,842
1089	27,817	1119	27,812	1149	28,201	1179	28,436	1209	28,281	1239	28,074	1269	28,354	1299	28,134	1329	28,021
1090	28,257	1120	28,224	1150	28,022	1180	28,018	1210	28,437	1240	28,076	1270	28,355	1300	27,909	1330	28,115
1091	28,38	1121	27,909	1151	28,096	1181	27,855	1211	28,284	1241	28,43	1271	28,081	1301	28,382	1331	28,374
1092	28,282	1122	27,886	1152	28,046	1182	28,176	1212	27,835	1242	25,591	1272	27,95	1302	28,222	1332	28,095
1093	23,1	1123	28,366	1153	28,058	1183	28,156	1213	28,107	1243	28,541	1273	28,426	1303	28,051	1333	28,126
1094	27,872	1124	27,905	1154	28,772	1184	28,366	1214	26,909	1244	28,144	1274	28,429	1304	26,945	1334	27,701
1095	28,232	1125	28,087	1155	28,343	1185	28,112	1215	28,35	1245	28,231	1275	26,569	1305	28,395	1335	28,113
1096	28,321	1126	28,397	1156	27,874	1186	27,954	1216	27,955	1246	28,331	1276	28,32	1306	28,169	1336	27,827
1097	28,383	1127	28,321	1157	28,245	1187	27,8	1217	28,072	1247	27,72	1277	28,214	1307	28,38	1337	28,139
1098	28,697	1128	28,255	1158	27,928	1188	28,334	1218	28,298	1248	28,126	1278	28,148	1308	28,054	1338	28,248
1099	28,092	1129	28,538	1159	28,195	1189	27,956	1219	28,107	1249	28,333	1279	28,107	1309	28,234	1339	27,813
1100	28,392	1130	28,1	1160	28,323	1190	28,204	1220	27,695	1250	28,294	1280	27,879	1310	28,233	1340	28,309
1101	28,451	1131	28,199	1161	28,4	1191	28,309	1221	28,26	1251	28,343	1281	28,281	1311	27,843	1341	28,395
1102	28,194	1132	27,512	1162	28,272	1192	28,321	1222	27,436	1252	28,451	1282	27,886	1312	28,063	1342	28,256
1103	28,209	1133	28,57	1163	27,618	1193	28,403	1223	28,006	1253	28,159	1283	28,273	1313	28,188	1343	28,306
1104	28,212	1134	28,175	1164	28,097	1194	28,246	1224	28,362	1254	27,885	1284	28,199	1314	28,385	1344	28,286
1105	28,132	1135	28,155	1165	28,444	1195	28,338	1225	28,105	1255	28,636	1285	28,161	1315	28,231	1345	27,893
1106	28,134	1136	27,799	1166	28,226	1196	28,219	1226	27,94	1256	28,218	1286	28,465	1316	27,292	1346	28,374
1107	27,504	1137	28,362	1167	28,267	1197	28,232	1227	28,243	1257	28,02	1287	27,868	1317	28,308	1347	28,025
1108	28,296	1138	27,77	1168	28,55	1198	27,961	1228	28,035	1258	27,715	1288	24,072	1318	27,893	1348	28,503
1109	28,199	1139	26,99	1169	28,047	1199	28,344	1229	28,451	1259	28,165	1289	27,976	1319	27,902	1349	28,131
1110	27,305	1140	28,348	1170	28,168	1200	27,863	1230	28,283	1260	26,928	1290	27,064	1320	28,232	1350	28,075

Figure 21 Raw data of the designed protein binders 1081 up until 1350 with their pAE interaction score, scored using AF2.

binder number	pae_interaction	binder number	pae_interaction	binder number	pae_interaction	binder number	pae_interaction	binder number	pae_interaction
1351	28,05	1381	28,144	1411	28,779	1441	28,53	1471	27,907
1352	28,381	1382	28,033	1412	27,816	1442	27,844	1472	28,306
1353	28,247	1383	28,328	1413	28,276	1443	28,234	1473	28,252
1354	28,386	1384	28,223	1414	28,427	1444	28,237	1474	28,025
1355	28,378	1385	28,438	1415	27,416	1445	28,15	1475	28,138
1356	27,786	1386	28,572	1416	28,028	1446	28,124	1476	28,086
1357	27,643	1387	28,075	1417	27,899	1447	27,688	1477	28,183
1358	27,966	1388	27,992	1418	28,314	1448	28,068	1478	28,234
1359	27,985	1389	28,057	1419	28,239	1449	28,377	1479	27,377
1360	27,74	1390	28,362	1420	28,035	1450	28,358	1480	28,238
1361	28,372	1391	28,065	1421	27,905	1451	28,124	1481	27,46
1362	28,411	1392	28,313	1422	28,305	1452	28,198	1482	27,999
1363	28,39	1393	28,412	1423	28,182	1453	28,205	1483	28,367
1364	27,428	1394	27,882	1424	28,229	1454	28,252	1484	28,764
1365	26,363	1395	28,174	1425	28,298	1455	28,537	1485	28,381
1366	28,13	1396	27,607	1426	28,046	1456	28,005	1486	27,956
1367	27,722	1397	28,322	1427	28,304	1457	28,103	1487	28,066
1368	28,453	1398	28,546	1428	27,98	1458	28,397	1488	28,066
1369	28,13	1399	27,694	1429	28,139	1459	27,402	1489	28,347
1370	28,4	1400	28,237	1430	28,207	1460	28,225	1490	28,484
1371	28,044	1401	28,228	1431	27,994	1461	28,451	1491	28,226
1372	28,223	1402	28,172	1432	28,279	1462	27,849	1492	28,131
1373	27,997	1403	28,476	1433	28,145	1463	27,972	1493	28,53
1374	28,262	1404	27,866	1434	28,268	1464	28,239	1494	27,807
1375	27,988	1405	28,189	1435	28,121	1465	28,16	1495	28,303
1376	28,457	1406	28,222	1436	28,109	1466	28,085	1496	28,189
1377	28,152	1407	28,373	1437	28,287	1467	28,457	1497	27,878
1378	28,205	1408	28,307	1438	28,302	1468	27,997	1498	28,034
1379	27,969	1409	27,896	1439	28,416	1469	27,981	1499	28,467
1380	28,359	1410	28,2	1440	28,189	1470	28,26	1500	28,123

Figure 22 Raw data of the designed protein binders 1351 up until 1500 with their pAE interaction score, scored using AF2.

Disclaimer; ChatGPT was used in order to improve my writing and correct for spelling errors in some parts of this bachelor thesis.